

PAPER • OPEN ACCESS

# From $\sqrt{3} \times \sqrt{3} R30^\circ$ -arsenene to $5 \times 5$ -arsenene on Ag(111): an atomic reversible phase transition

To cite this article: Paola De Padova *et al* 2025 *2D Mater.* **12** 025018

View the [article online](#) for updates and enhancements.

You may also like

- [Termination-dependent electronic structure and atomic-scale screening behavior of the  \$\text{Cu}\_2\text{O}\(111\)\$  surface](#)  
Alexander Gloystein, Niklas Nilius, Claudine Noguera et al.
- [Evidence of new 2D material:  \$\text{Cu}\_2\text{Te}\$](#)   
Yongfeng Tong, Meryem Bouaziz, Wei Zhang et al.
- [Dissolution suppression of self-assembled GaSb quantum dots on silicon by proper surface preparation](#)  
Dmitriy Goroshko, Evgeniy Chusovitin, Evgeniy Subbotin et al.



## PAPER

## OPEN ACCESS

## RECEIVED

4 November 2024

## REVISED

29 December 2024

## ACCEPTED FOR PUBLICATION

21 January 2025

## PUBLISHED

7 February 2025

Original content from this work may be used under the terms of the [Creative Commons Attribution 4.0 licence](https://creativecommons.org/licenses/by/4.0/).

Any further distribution of this work must maintain attribution to the author(s) and the title of the work, journal citation and DOI.



# From $\sqrt{3} \times \sqrt{3} R30^\circ$ -arsenene to $5 \times 5$ -arsenene on Ag(111): an atomic reversible phase transition

Paola De Padova<sup>1,2,\*</sup> , Carlo Ottaviani<sup>1</sup> , Bruno Olivieri<sup>3</sup>  and Mariusz Krawiec<sup>4</sup> <sup>1</sup> Consiglio Nazionale delle Ricerche-ISM, Via Fosso del Cavaliere 100, 00133 Roma, Italy<sup>2</sup> INFN-LNF, Via Enrico Fermi 54, 00044 Frascati (Roma), Italy<sup>3</sup> Consiglio Nazionale delle Ricerche-ISAC, Via Fosso del Cavaliere 100, 00133 Roma, Italy<sup>4</sup> Institute of Physics, Maria Curie-Skłodowska University, pl. M. Curie-Skłodowskiej 1, Lublin 20-031, Poland

\* Author to whom any correspondence should be addressed.

E-mail: [paola.depadova@ism.cnr.it](mailto:paola.depadova@ism.cnr.it)

**Keywords:** phase transition from 2D  $\sqrt{3} \times \sqrt{3} R30^\circ$ -arsenene to  $5 \times 5$ -arsenene,  $5 \times 5$ -arsenene, Auger electron spectroscopy, low energy electron diffraction, first-principles calculations, density functional theory

## Abstract

Two dimensional (2D)  $\sqrt{3} \times \sqrt{3} R30^\circ$ -As, has been discovered on Ag(111)  $1 \times 1$  surface, by depositing 1 monolayer of As, keeping the silver substrate at a temperature of  $\sim 450^\circ\text{C}$ , while a  $2\text{D } 5 \times 5$  reconstruction, attributed to arsenene, appeared at a lower temperature of  $\sim 350^\circ\text{C}$ . The two  $\sqrt{3} \times \sqrt{3} R30^\circ$ -As and  $5 \times 5$ -arsenene surface reconstructions were experimentally investigated by means of low electron energy diffraction, and Auger electron spectroscopy, while the first-principles calculations, by using density functional theory, confirmed their atomic configurations, surface stability, and the prediction that the  $\sqrt{3} \times \sqrt{3} R30^\circ$ -As reconstruction, can be considered as a new allotropic form of arsenene, exhibiting electronic structure with metallic character. A reversible structural phase transition, from the  $2\text{D } \sqrt{3} \times \sqrt{3} R30^\circ$ -arsenene to the  $5 \times 5$ -arsenene surface reconstruction, induced by electron-beam irradiation, and recovered to the  $\sqrt{3} \times \sqrt{3} R30^\circ$ -As, by annealing, was observed, opening a new path to study reversible phase transitions in elemental epitaxial 2D materials.

## 1. Introduction

Arsenic (As), along with phosphorus (P) antimony (Sb), and bismuth (Bi), belongs to the nitrogen (N) group, the fifteenth group of the periodic table, whose elements are called, more specifically, pnictogens, referring to the suffocating properties of N, that is, the opposite of the action of oxygen.

Another peculiar property of pnictogen atoms is that they act as surfactants, given their ability to float on top of surfaces, in epitaxial growths, in particular those containing Ge and Si. Thus, As, Sb, and Bi have long been successfully used, in the past, for example as an intercalating layer for strained epitaxial growths of germanium on the Si(001) surface [1].

Right, moving one column to the left of the periodic table, we fall back to the fourteenth column, encountering the element carbon (C), entered into the limelight, with the discovery of graphene [2], single C atom thick in a honeycomb lattice, like its

natural allotropic form, the graphite, in the two-dimensional (2D) arrangement.

Subsequently, the new synthetic allotropic form of silicon (Si) was discovered [3], opening the way to synthesize and study the elemental 2D materials with the suffix -ene, which, under given specific synthesis conditions, can take on a honeycomb-type lattice. For silicon a buckled [3], and a flat [4] honeycomb lattice were found.

Right now, regarding the issue of elemental 2D materials, numerous systems have been discovered to exhibit an honeycomb-like atomic arrangement, such as, for example, for group-IVA, germanene supported, up to now, on several substrates, such as Ag(111) [5], Cu(111) [6], MoS<sub>2</sub> [7], Al(111) [8], Ge<sub>2</sub>Pt [9], Au(111) [10], and Pt(111) [11]; stanene on Bi<sub>2</sub>Te<sub>3</sub>(111) [12], and Cu(111) [13], as well as Plumbene on Pd(111) [14], and Ir(111) [15]; for group VA, blue phosphorene on Au(111) [16], arsenene on Ag(111) [17], ultrathin film of Sb(111)

(antimonene) was performed on  $\text{Bi}_2\text{Te}_3$  and  $\text{Sb}_2\text{Te}_3$  substrates [18] by molecular beam epitaxy, and later on  $\text{PdTe}_2$  [19], bismuthene on SiC substrate obtained by epitaxial growth [20]; for group IVB, hafnene [21]; for group IIIA, borophene [22–24], gallenene [25]; for group VIA, selenene [26], and tellurene [27]. In addition, it should be noted that, recently, more and more new 2D material systems, such as transition metal halide  $\text{ZrX}_2$  ( $X = \text{Cl, Br, I}$ )/ $\text{Zr}_2\text{Cl}_2$  van der Waals heterojunctions, and 2D half-semiconducting material  $\text{Mn}(\text{BiTeS})_2$ , with very intriguing physical properties, have been proposed [28, 29].

Several authors have theoretically predicted [30–34] that elemental As, Sb and Bi, the heavy pnictogens, could exhibit stable single-layered materials derived from bulk gray arsenic, gray antimony, and bismuth and then called arsenene (h-As), antimonene (h-Sb) [30–32, 35] and bismuthene (h-Bi) [34]. They crystallize in the rhombohedral layered structure (space group  $R\bar{3}m$ ), named  $\beta$ -phase, which is their most stable allotrope, although natural bulk As and Sb have other allotropic structures, even if considered metastable [36, 37].

*Ab initio* DFT calculations of thin film layered gray As showed the equilibrium geometry with electronic properties, exhibiting large band gap, at variance of a semi-metallic behavior, of bulk gray As [30, 38]. The electronic properties can be affected by several factors, for instance, the number of layers, comprising interlayer distance and/or the compressive/tensile strains [30], where strain mainly was found to induce metal-semiconductor transition, in monolayers (MLs) and bilayers of gray arsenic [30]. These results were confirmed by [31], where, again, first-principles DFT calculations, reported that arsenene could arrange two stable types of honeycomb structures, the buckled- and the puckered-type, with both arsenene structures keeping indirect gaps, also modified by strain. Recently, interesting enough, a new first-principles DFT calculations have been used to investigate the arsenene electronic structures and topological phase transition under tensile and compressive strains [39].

Again, atomically thin arsenene and antimonene were identified as two novel wideband gap semiconductors, with very stable honeycomb structure, from bulk to ML transition, followed by semimetal–semiconductor with large indirect band-gap transitions [40].

Nevertheless, more recently, 2D group-VA semiconductors, both from theory and experiment have been revisited [35], expanding, with success, the family of the so-called Dirac materials. In meanwhile, nanosheets and nanodots of 2D arsenene were achieved by the ultrasonication of grey arsenic in such proper solvents [41], as well as the growth of this  $\beta$ -phase arsenic bulk crystals, i.e. the rhombohedral layered structure (space group  $R\bar{3}m$ ), were also

obtained, via chemical vapor transport method, from which their large-scale nanoflakes were employed, for the first time, to achieve an interesting near-infrared pulsed laser for nonlinear photonic applications [42].

The experimental evidence, of one ML of arsenene, synthesized on the  $\text{Ag}(111)1 \times 1$  single crystal, kept in the temperature range between 250 and 350 °C, was achieved, adopting the honeycomb  $5 \times 5$  reconstruction [17]. It is worth mentioning another system, involving As/Ag(111), which consists of a one-dimensional structure formed by  $\text{Ag}_2\text{As}$  surface alloy [43]. The experimental conditions for achieving this surface alloy were just to anneal  $\text{Ag}(111)5 \times 5$ -As at a temperature of  $\sim 400$  °C in front of the low electron energy diffraction (LEED) optics until diffraction spots appeared [43]. A fairly complicated LEED pattern was found for this As/Ag(111) striped phase: the  $\text{Ag}(111)1 \times 1$  spots are surrounded by six satellite spots; surrounding the  $\sqrt{3} \times \sqrt{3}$  classical positions, there were six spots forming triangles. Between the triangles there were seven diffraction spots. Note that there were no diffraction spots at the  $\sqrt{3} \times \sqrt{3}$  positions, which makes the reconstruction recognized as formed by an approximate  $14\sqrt{3}$  ( $\sqrt{3} \times 14$ ) periodicity [43].

The present work specifically focusses on the formation and investigation of the electronic and structural properties of the 2D antimonene phase on  $\text{Ag}(111)1 \times 1$ , exhibiting the  $5 \times 5$  surface reconstruction, and the  $\text{Ag}(111)\sqrt{3} \times \sqrt{3} R30^\circ$ -As interface. This last phase undergoes the transition to the previous reconstruction (2D arsenene  $5 \times 5$ ), when applying an  $e^-$  irradiation on the surface. Reversibly, the  $\text{Ag}(111)\sqrt{3} \times \sqrt{3} R30^\circ$ -As reconstruction can be regained by annealing the 2D arsenene/Ag interface, again. Density functional theory (DFT) confirms these results, providing interesting electronic features, through band dispersion calculations.

## 2. Experimental

The experiments were performed at the CNR-ISM laboratories of Tor Vergata, Rome (Italy), and the theoretical part was computed at the Institute of Physics, Maria Curie-Skłodowska University, Lublin (Poland). LEED patterns were acquired at primary energy ( $E_p$ ) ranging from  $\sim 39$  eV up to 135 eV, while the AES spectra, in first derivative mode, were recorded at a primary electron beam of ( $E_p = 3.0$  KeV) from the coaxial e-gun in the PHI 255 G double-pass cylindrical mirror analyzer, CMA, exhibiting at least 0.5 eV of resolution. The  $\text{Ag}(111)$  single crystal was cleaned, in the UHV chamber (base pressure:  $2.0 \cdot 10^{-10}$  mbar), by repeated cycles of sputtering and annealing up to 450 °C, in order to achieve a clear ordered LEED pattern from the  $\text{Ag}(111)1 \times 1$  unreconstructed surface.

As was evaporated on Ag(111)1 × 1 kept in the range of  $T_{\text{sub}} = (250\text{--}350)^\circ\text{C}$ , and at  $T_{\text{sub}} = 480^\circ\text{C}$ , adopting a rate of  $\sim 0.08\text{ ML min}^{-1}$  from an As solid source up to  $\sim 1\text{ ML}$ . The Ag(111)5 × 5-As reconstruction, here called arsenene, was obtained in the first case, and the Ag(111) $\sqrt{3} \times \sqrt{3}$ -As reconstruction, in the second. The surface irradiation by AES e-beam of As/Ag(111) interface, was performed by applying a current of  $\sim 0.2\text{ mA}$  for several hours.

The DFT calculations were performed using the Perdew–Burke–Ernzerhof (PBE) [44] implementation of the generalized gradient approximation (GGA), as implemented in Vienna ab initio simulation package (VASP) [45, 46]. The electron-ion interaction was described with the projector-augmented wave method [47]. The plane wave energy cut-off for all calculations was set at 340 eV, and the Brillouin zones associated with the Ag(111)5 × 5-As and Ag(111) $\sqrt{3} \times \sqrt{3}$ -As unit cells were sampled by  $3 \times 3 \times 1$  and  $9 \times 9 \times 1$  Monkhorst–Pack  $k$ -points grids, respectively [48]. The Ag(111)–As system has been modeled by five Ag layers and the reconstruction Sb layer. A vacuum region of 17 Å has been added to avoid the interaction between surfaces of the slab. All atomic positions were relaxed, except the bottom layer, until the largest force in any direction was below  $0.01\text{ eV \AA}^{-1}$ . The Ag atoms in the bottom layer were fixed at their ideal bulk positions.

### 3. Results and discussion

Figure 1 describes the growth behavior of the Ag(111)5 × 5-As system. For this reason it is imperative to identify the coverage of 1 ML of As, which forms the arsenene layer, keeping the substrate temperature at  $250^\circ\text{C}$  [17].

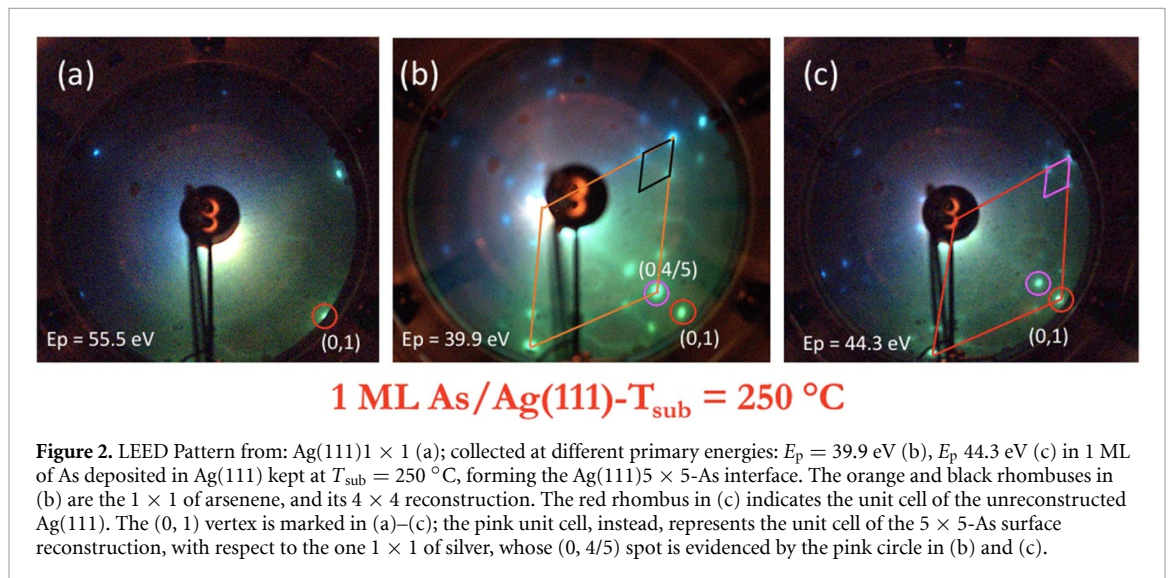
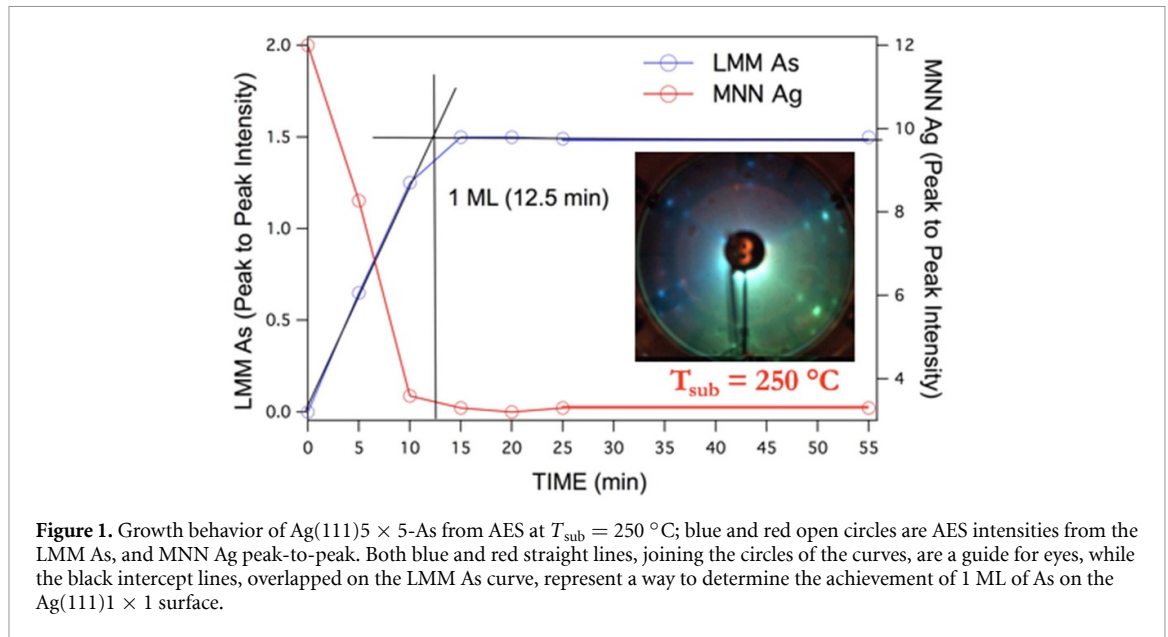
Therefore, the figure 1 reports the growth behavior of Ag(111)5 × 5-As obtained from the LMM As, and MNN Ag peak-to-peak AES intensities, keeping the substrate temperature at  $T_{\text{sub}} = 250^\circ\text{C}$ . The blue and red open circles are from the LMM As, and MNN Ag peak-to-peak AES intensities, at the left and right vertical axes, respectively, whereas the straight lines, joining the circles of the curves, are a guide for eyes. The vertical black line, represents a way to determine the achievement of 1 ML of As on the Ag(111)1 × 1 surface, obtained after 12.5 min of deposition. It is worth noting that the AES Ag MNN and As LMM lineshapes for all As growth (up to about 4.4 MLs) were similar, (spectra not shown) and that after the adsorption of 1 ML of As, no further atom uptake was found, as attested by the constant As and Ag peak-to-peak AES intensities, after the appearance of the elbow of the curve.

Let us show now in figure 2(a) the typical LEED pattern of the single crystal Ag(111)1 × 1 unreconstructed surface, while the patterns after the deposition of 1 ML of As, keeping the substrate at temperature of  $T_{\text{sub}} = 250^\circ\text{C}$ , are shown in figures 2(b) and (c), collected at primary electron beam energies,  $E_p$ , of 55.5 eV; 39.0 eV; and 43.3 eV respectively. The Ag(111)5 × 5-As surface reconstruction, formed by one layer of arsenene, is clearly visible in figures 2(b) and (c), in nice agreement with [17]. The red, and pink open circles in figures 2(b) and (c) represent the (0, 1), and (0, 4/5) spots of Ag(111)1 × 1 and Ag(111)5 × 5-As. The 4 × 4 reconstruction of arsenene with respect to its own 1 × 1, is marked, in figure 2(b), by black, and orange rhombus, respectively, while the red rhombus characterizes the 1 × 1 unit cell of the unreconstructed Ag(111), figure 2(c). The smaller units cell, i.e. the pink rhombus in figure 2(c), is that of the Ag(111)5 × 5-As reconstructions, with respect to the Ag(111)1 × 1.

Taking advantage of the fact that the Ag(111)5 × 5-As was found in the range of  $T_{\text{sub}} = (250\text{--}350)^\circ\text{C}$  [17], the temperature stability of 1 ML of arsenene on Ag(111) was probed by increasing the temperature up to  $320^\circ\text{C}$ , in front of LEED system, as shown in figure 3. LEED patterns were collected at several  $E_p$  energies, figures 3(a)–(d), from lowest, such as 36.5 eV to highest, 117.1 eV, obtained maintaining the  $5 \times 5/4 \times 4$  reconstruction of arsenene.

Continuing to raise the temperature, around  $T_{\text{sub}} = 350^\circ\text{C}$  the Ag(111)5 × 5-As reconstruction begins to become confused, giving way to another surface order, identified as Ag(111) $\sqrt{3} \times \sqrt{3}$ -As, which at  $T_{\text{sub}} = 480^\circ\text{C}$ , clearly manifests itself. Figure 4 reports the LEED patterns, obtained from 1 ML of As deposited on the Ag(111) surface, keeping the substrate directly at  $T_{\text{sub}} = 480^\circ\text{C}$ . In order to well recognize the Ag(111) $\sqrt{3} \times \sqrt{3}$ -As, LEED patterns at different  $E_p = 48.5\text{ eV}$  (a),  $E_p = 59.4\text{ eV}$  (b), and  $E_p = 135.4\text{ eV}$  (c) are shown in figures 4(a)–(c). The red rhombus in (a) indicates the unit cell of the unreconstructed Ag(111); the (0, 1) vertex is marked in (b), while the yellow one represents the unit cell of the  $\sqrt{3} \times \sqrt{3}$ -As surface reconstruction, rotated  $30^\circ$  with respect to that of the unreconstructed silver. One of the (1/3,1/3) spot of the Ag(111) $\sqrt{3} \times \sqrt{3}$ -As is evidenced by the yellow circle in (b).

It is extremely important to note that this is the first time that a 2D layer of As on Ag(111) surface, having a  $\sqrt{3} \times \sqrt{3}$  reconstruction, considered here as pure  $\sqrt{3} \times \sqrt{3}$ , has been identified, to be distinguished from the more complicated one found, recently, in [43], after the annealing of the Ag(111)5 × 5-arsenene at temperature of  $\sim 400^\circ\text{C}$  up to some diffraction spots  $\sqrt{3} \times \sqrt{3}$ -like appeared on the LEED pattern, and attributed to a peculiar As/Ag



surface alloy. In addition, various diffraction spots were there observed, such as six satellites spots, forming an hexagon around each  $1 \times 1$  spots of Ag(111); surrounding each ideal  $\sqrt{3} \times \sqrt{3}$  position, a group of six spots, creating triangles, plus some extra spots just next to the triangles, were probed, and, furthermore, rows of seven closely spaced diffraction spots between the triangles were located, with three different orientations, indicating that three reconstruction domains were present on the surface. Exactly at the  $\sqrt{3} \times \sqrt{3}$  positions, no diffraction spots were found, showing a substantial deviation from that simple periodicity [43], found, instead, interestingly, in our work.

This points out to the first time that the Ag(111) $\sqrt{3} \times \sqrt{3} R30^\circ$ -As interface was observed.

Under the  $e^-$  irradiation emitted by the electron gun of the AES electron energy analyzer (PHI 255 G, double-pass CMA), with a primary energy of

$E_p = 2.5 \text{ keV}$ , at  $\sim 0.2 \text{ mA}$ , and for a time of several hours, the Ag(111) $\sqrt{3} \times \sqrt{3} R30^\circ$ -As interface transforms back into the Ag(111) $5 \times 5$ -As reconstruction. The LEED pattern attesting this phase transition, is shown in figure 5, where the As-( $4 \times 4$ )/( $5 \times 5$ ) (the  $4 \times 4$  being considered with respect to the  $1 \times 1$  unit cell of arsenene) is collected at two primary energies of 48.3 eV and 31 eV. The arrows indicate the  $\times 4$ , and  $\times 5$ , reconstructions.

Sometimes, the using of electron beams to analyze the chemical and stoichiometry composition of solids could modify, and/or damage the samples under investigation. Much more clearly, biological and organic materials, but also metallic, ionic, and inorganic materials can suffer from electron beam damaging [49]. In the case of electron microanalysis/microscopy and transmission electron microscopy, where both high energy electron beam and

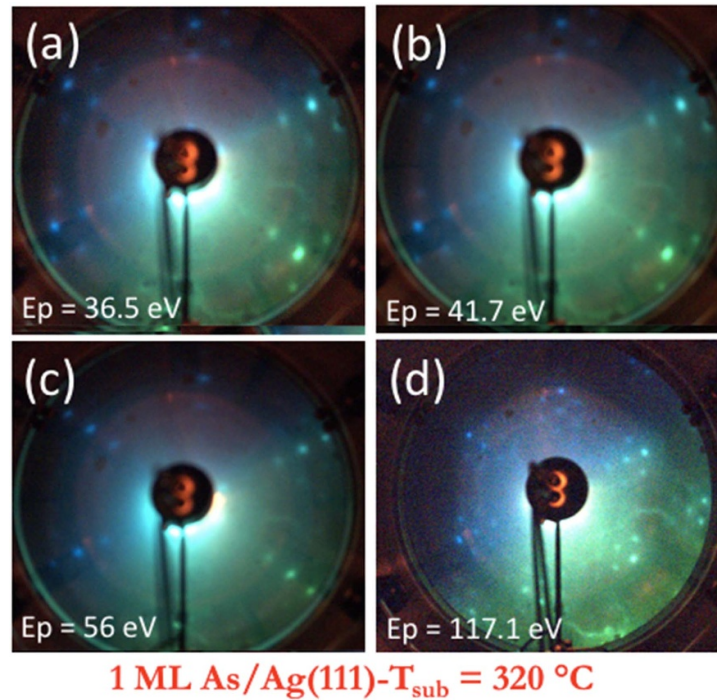


**Figure 3.** LEED pattern from 1 ML of As deposited on Ag(111) kept at  $T_{\text{sub}} = 320\text{ }^{\circ}\text{C}$ , forming the Ag(111) $5 \times 5$ -As interface: Ag(111) $1 \times 1$  (a) collected at different primary energy  $E_p = 36.5\text{ eV}$  (a),  $E_p = 41.7\text{ eV}$ (b),  $E_p = 56\text{ eV}$  (c), and  $E_p = 117.1\text{ eV}$  (d).

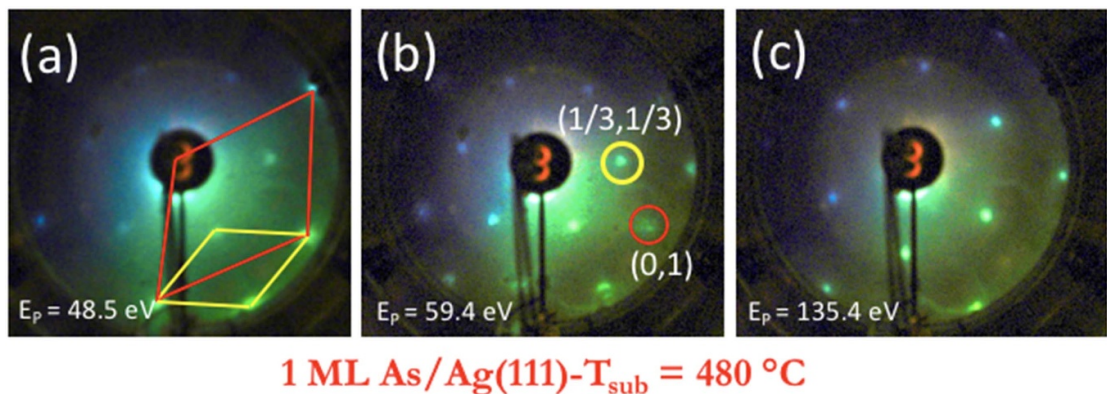


**Figure 4.** LEED patterns collected at different primary energy (a) ( $E_p = 48.5\text{ eV}$ ), (b) ( $E_p = 59.4\text{ eV}$ ), (c) ( $E_p = 135.4\text{ eV}$ ) on 1 ML of As deposited on Ag(111) kept at  $T_{\text{sub}} = 480\text{ }^{\circ}\text{C}$ , forming the Ag(111) $\sqrt{3} \times \sqrt{3}R30^{\circ}$ -As interface. The red rhombus in (a) indicates the unit cell of the unreconstructed Ag(111), the (0, 1) vertex is marked (b); while the yellow one represents the unit cell of the  $\sqrt{3} \times \sqrt{3}$ -As surface reconstruction; one of the (1/3,1/3) spot is evidenced by the yellow circle (b).

high current density are applied, not only the surface, but more properly the bulk of samples can be affected by the electron beam damage [49].

AES is a surface-sensitive technique. An electron beam damage, which can affect the samples surface in several ways, can influence the AES spectra, often, presenting the effects all together. Changes in chemical composition and/or stoichiometry, lattice or other structural modification/distortion, production or elimination of defects, and/or electrical charging were reported [49].

Two main processes, called electronic stimulated desorption (ESD), and electronic stimulated adsorption (ESA), can occur during an AES measurement, and/or electron gun irradiation.

ESD can be considered as a composite process, involving the electronic excitation of chemical species at the surface, producing the escape of the excited fragments, or their de-excitation and recapturing upon the surface [49].

The ESA process can be due to electronic excitation or a molecule dissociation of a gas phase at the

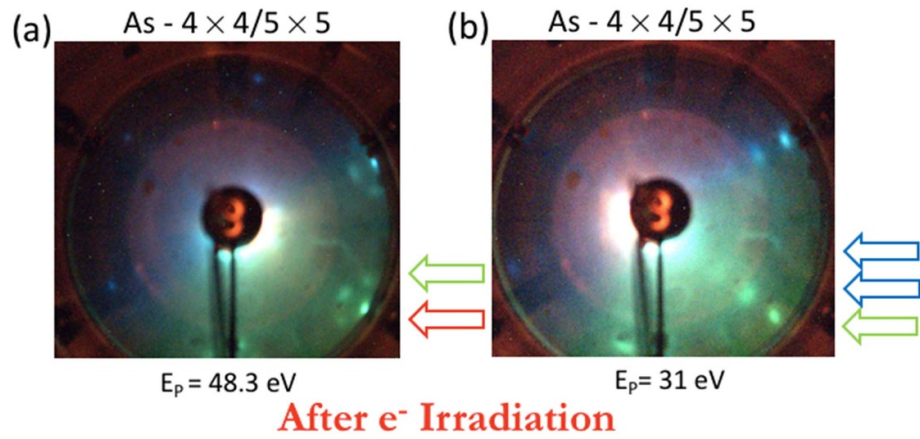


**Figure 5.** LEED patterns of arsenene on Ag(111) at 48.3 eV (a) collected after  $e^-$  irradiation for several hours of the As/Ag(111) $\sqrt{3} \times \sqrt{3}$ . The red arrow indicates one of the integer Ag(1  $\times$  1) spots, while an arsenene spot of the 5  $\times$  5 reconstruction with respect to the Ag(111)1  $\times$  1 is indicated by the green arrow. In (b) the LEED pattern at 31 eV shows the arsenene 4  $\times$  4 (blue arrows) with respect to the arsenene 1  $\times$  1 (green arrow).

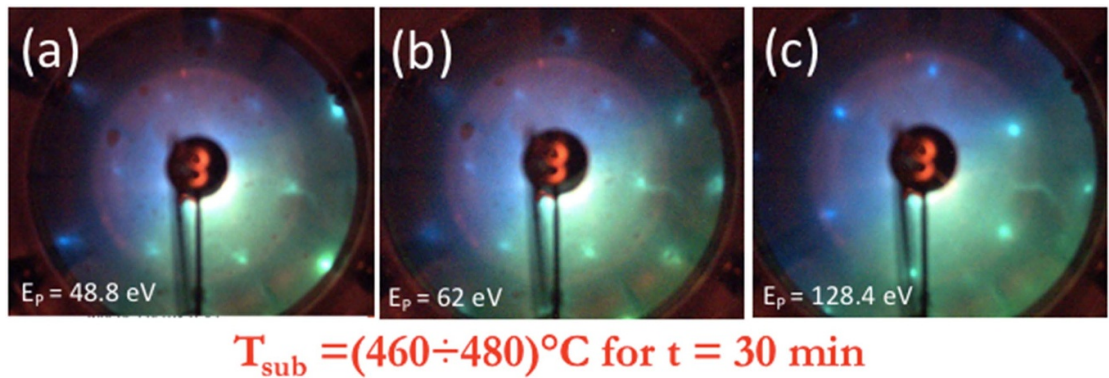


**Figure 6.** LEED patterns collected at different primary energies (a) ( $E_p = 48.8$  eV), (b) ( $E_p = 62$  eV), (c) ( $E_p = 128.4$  eV) on 1 ML of As on the Ag(111) $\sqrt{3} \times \sqrt{3}$  R30 $^\circ$ -As interface, obtained by the transition of the Ag(111)5  $\times$  5-As interface of figure 5 upon annealing at  $T = (460 \div 480)^\circ\text{C}$  for  $t = 30$  min.

surface, or of a molecule weakly bonded to the surface [49].

Thus, the interaction between an electronically excited atom, or molecule, and a surface, can induce adsorption and reaction at the surface.

Unfortunately, in our particular case, we cannot clearly distinguish between ESD and ESA, finding ourselves faced with a structural phase transition between arsenene-(5  $\times$  5), and As/Ag(111) $\sqrt{3} \times \sqrt{3}$ .

The Ag(111)5  $\times$  5-arsenene layer, obtained after AES electron gun irradiation, was then annealed again at temperatures between (460  $\div$  480) $^\circ\text{C}$  for  $t = 30$  min. It is interesting noting that the previous reconstruction, Ag(111) $\sqrt{3} \times \sqrt{3}$  R30 $^\circ$ -As, is gained again, as demonstrated by the LEED patterns of figure 6, at different primary energy:  $E_p = 48.8$  eV (a);  $E_p = 62$  eV (b), and  $E_p = 124.8$  eV (c).

This important result is a clear demonstration of the reversible structural phase transition that occurs on the As/Ag(111) interface.

At this point it is worth showing that the intensity of the AES signals, namely Ag MNN and As LMM

are similar both in intensity and shape, as it can be immediately seen in figure 7, which shows the comparison between the two Ag(111)5  $\times$  5-As, and Ag(111) $\sqrt{3} \times \sqrt{3}$  R30 $^\circ$ -As phases obtained, the first, after the  $e^-$  irradiation of the Ag(111) $\sqrt{3} \times \sqrt{3}$  R30 $^\circ$ -As reconstruction, and, the second, after a surface re-annealing at temperature  $T_{\text{sub}} = 480$   $^\circ\text{C}$ .

This result is very important since it supports our hypothesis of being able to pass from one phase to another for the As/Ag(111) interface, both by changing the temperature of the substrate and by the surface irradiation with the AES  $e^-$  electron gun.

In order to summarize the experimental results shown, figure 8 reports a graphical description of the driving force, temperature and  $e^-$  gun irradiation, inducing the reversible phase transition between the two 5  $\times$  5 and  $\sqrt{3} \times \sqrt{3}$  R30 $^\circ$  arsenene surface structures, in its reversible atomic-assembling process. Three simple steps, clarify the mechanism: (1) in the range of temperature between 250  $^\circ\text{C}$  and 320  $^\circ\text{C}$  the 5  $\times$  5 arsenene reconstruction takes over, leaving the place to the  $\sqrt{3} \times \sqrt{3}$  R30 $^\circ$  arsenene reconstruction

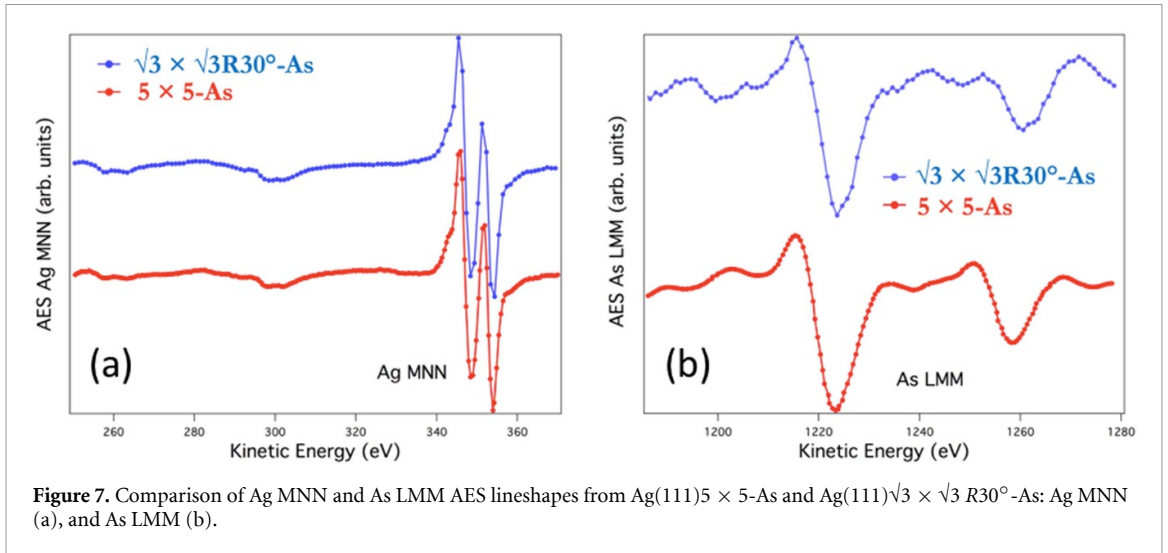


**Figure 7.** Comparison of Ag MNN and As LMM AES lineshapes from Ag(111) $5 \times 5$ -As and Ag(111) $\sqrt{3} \times \sqrt{3} R30^\circ$ -As: Ag MNN (a), and As LMM (b).

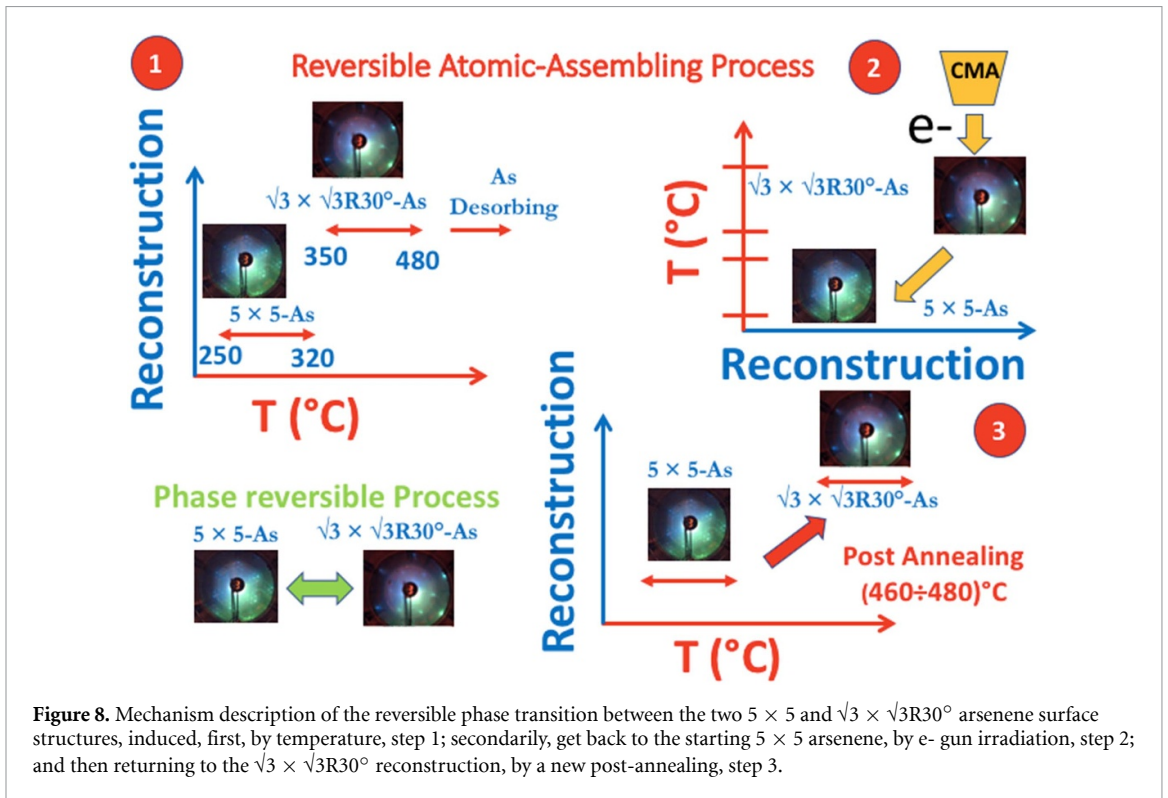


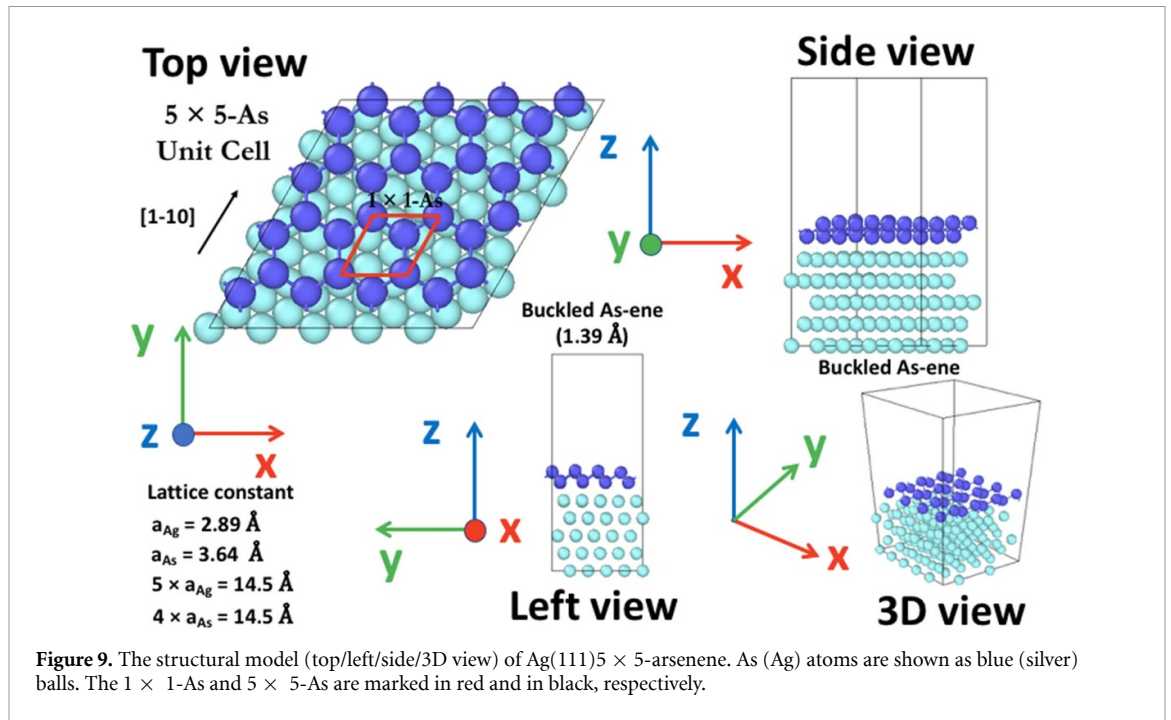
**Figure 8.** Mechanism description of the reversible phase transition between the two  $5 \times 5$  and  $\sqrt{3} \times \sqrt{3} R30^\circ$  arsenene surface structures, induced, first, by temperature, step 1; secondarily, get back to the starting  $5 \times 5$  arsenene, by e- gun irradiation, step 2; and then returning to the  $\sqrt{3} \times \sqrt{3} R30^\circ$  reconstruction, by a new post-annealing, step 3.

at higher temperatures comprise into 350 °C and 480 °C, where the onset of As desorbing process begins. In step 2, the Auger e-gun irradiation, promotes the returning back to the original  $5 \times 5$  arsenene reconstruction, which can settle again to  $\sqrt{3} \times \sqrt{3} R30^\circ$ -As, in step 3, after applying a new post-annealing, at temperature range of (460–480) °C.

To shed more light on our experimental findings, we carried out first-principles DFT calculations of As on Ag(111). In the case of As-( $5 \times 5$ )/Ag(111) system, the As layer acquires the characteristic form of a free-standing arsenene. The obtained structural parameters, i.e. the lattice constant  $a_{As} = 3.64 \text{ \AA}$  and the buckling  $d = 1.39 \text{ \AA}$ , agree well with their free-standing values 3.55–3.61 Å and 1.35–1.45 Å, respectively [17].

This, together with large As-Ag(111) surface separation, which yields 3.34 Å, and low binding energy,  $E_b = 380 \text{ meV}$  per As atom, allows us to think of the As-( $5 \times 5$ ) layer as (almost) freestanding arsenene, in agreement with [17]. The structural model is shown in figure 9. It corresponds to the As surface coverage  $\vartheta = 1.28 \text{ ML}$ , where 1 ML refers to the Ag(111) plane.

The lowest energy structural model of the Ag(111) $\sqrt{3} \times \sqrt{3} R30^\circ$ -As with approximately the same As surface coverage (now  $\vartheta = 1.33 \text{ ML}$ ), is shown in figure 10. Atoms in this new single-layer epitaxial As structure occupy three different vertical positions, separated by 0.90 Å, and 0.85 Å, respectively. Owing to the large distance to the surface, 3.17 Å,



and very low binding energy  $E_b = 170 \text{ meV}$ , this As layer can also be considered as weakly interacting with substrate.

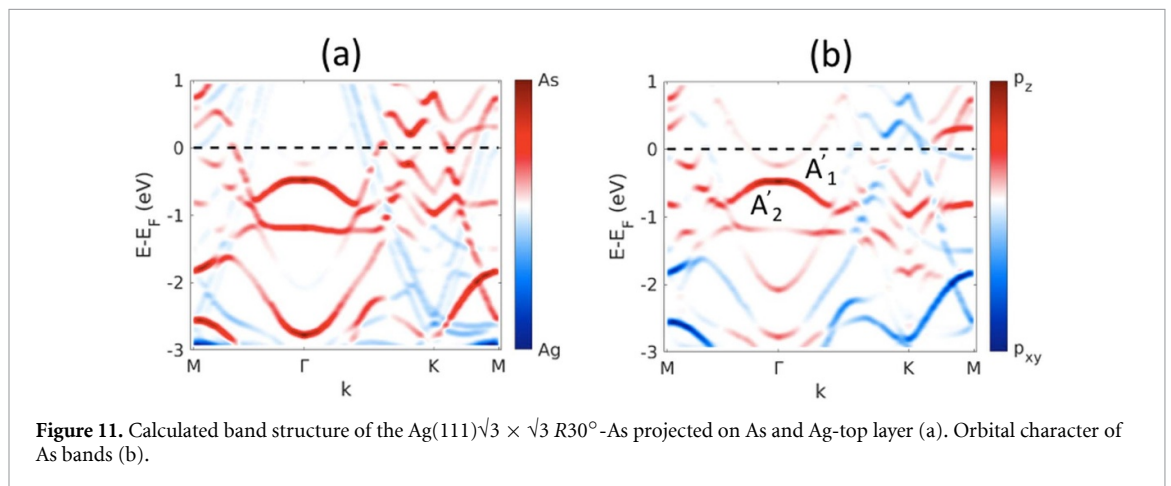
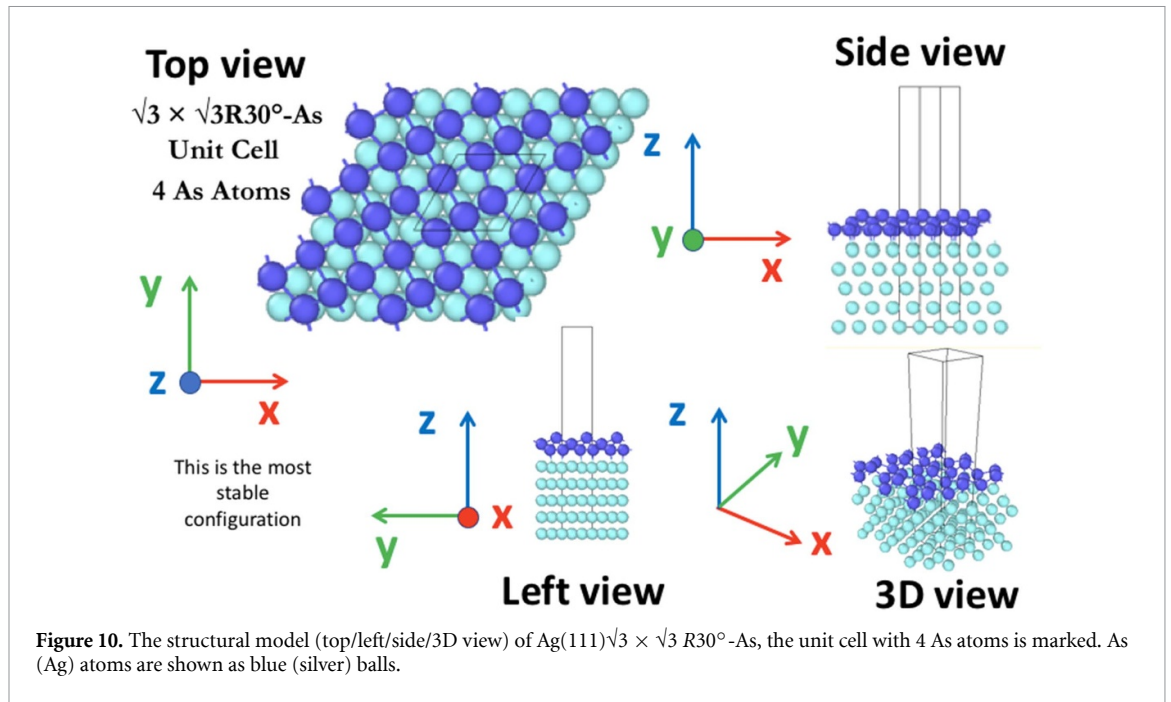
The weakly-interacting character of the  $\sqrt{3} \times \sqrt{3}R30^\circ$ -As layer is also reflected in electronic structure. Figure 11(a) shows the calculated band structure of the Ag(111) $\sqrt{3} \times \sqrt{3}R30^\circ$ -As projected on As and Ag-top layers, respectively. Clearly, system is metallic with a number of parabolic bands centered at the  $\Gamma$  point. They are composed mainly of the As  $4p_z$  orbitals, although the  $p_{xy}$  character is also visible for larger values of  $k$ , figure 11(b). There are also two well resolved additional bands with very strong As  $4p_z$  character: a hole-like band with its top edge around  $E = -0.5 \text{ eV}$ , and the flat band located around  $E = -1.2 \text{ eV}$ , named  $A_1$  and  $A_2$ . They resemble the  $A_1$  and  $A_2$  bands of the free-standing arsenene [17]. The As-Ag hybridization is visible mainly in the  $\Gamma$ -centered parabolic bands with their bottoms at energies equal to  $-0.2 \text{ eV}$  and  $-2.1 \text{ eV}$ .

The  $\sqrt{3} \times \sqrt{3}R30^\circ$ -As, being a single layer, can be regarded as a new allotropic form of arsenene. Unfortunately, this structure is unstable in the isolated form, and may exist only when supported. In a ‘real-world’ this structure can be used, for instance, embedded in a multilayer heterostructure, overcoming and/or stabilizing its new As reconstruction. On the other hand, As is not new in terms of metastability, as can easily be commented in the case of other allotropic forms of arsenic [36, 37]. Indeed, the yellow (non-metallic) forms of As (Sb) are metastable, they are prepared by condensing the vapor at very

low temperature; arsenic also forms a polymorph isostructural with black phosphorus [50, 51], obtained by simple heating amorphous As at  $100 \text{ }^\circ\text{C}$ – $175 \text{ }^\circ\text{C}$ , in presence of mercury [37]. By heating and/or exposing to light, the yellow form reverts to the metallic form [37], showing, mainly, its metastable behavior.

Thus, in principle, one can think of this new structure as kind of epitaxial arsenene, the counterpart of well-known  $\beta$ -arsenene, with metallic electronic properties [40]. Whether this structure can also be stabilized by other substrates is unknown at present.

According to the DFT calculations the  $\sqrt{3} \times \sqrt{3}R30^\circ$ -As shown in figure 10 is a potential candidate for the real atomic structure that we deal with in our experiments. Energetically, it is not far from the lowest energy Ag(111)5 × 5-arsenene structure, thus possible to be realized in the nature. From the experimental point of view, it is reasonable to assume that  $\sqrt{3} \times \sqrt{3}R30^\circ$ -As has the higher total energy than the 5 × 5-arsenene, and should be treated as a kind of metastable structure. This would explain why some extra energy (in the form of annealing) is required to drive 5 × 5-arsenene to the  $\sqrt{3} \times \sqrt{3}R30^\circ$ -As, and only some external factor, that causes the system to leave this local energy minimum and go back to the original 5 × 5-arsenene phase. Unfortunately, this driving force is unknown. We already discussed that AES e-gun can trigger various surface processes, and the interpretation of them can be extremely complex and often ambiguous. Nevertheless, one



possible scenario can be proposed. It concerns the physics behind the Auger effect and charge doping. This would be clear, if one recalls the final state of an atom after Auger event, which is hole-doped. Thus one should expect, that the  $\sqrt{3} \times \sqrt{3} R30^\circ$ -As structure might be hole-doped when AES e-gun is operating. This would trigger the transition to the original  $5 \times 5$ -arsenene phase. If this is true, it should be reflected in DFT calculations. Indeed, the DFT calculations show that the most stable structure is the  $5 \times 5$ -arsenene, while the  $\sqrt{3} \times \sqrt{3} R30^\circ$ -As is the metastable phase. What is more important, the  $\sqrt{3} \times \sqrt{3} R30^\circ$ -As is more likely realized at negative charge (electron) doping, while the  $5 \times 5$ -arsenene—at positive (hole) doping, as figure 12 reveals. That means that when electrons are subtracted from the  $\sqrt{3} \times \sqrt{3} R30^\circ$ -As, the system should evolve to the  $5 \times 5$ -arsenene, as observed

experimentally. Thus, the most likely driving force for this phase transition is charge doping.

#### 4. Conclusions

Two atomic structural phases have been discovered for the growth of As/Ag(111) interface, as a function of substrate temperature and Auger electron beam irradiation: the  $\text{Ag}(111)5 \times 5$ -arsenene, and the new allotropic form of arsenene, the  $\text{Ag}(111)\sqrt{3} \times \sqrt{3} R30^\circ$ -arsenene surface reconstructions, as demonstrated by AES, LEED, and DFT calculations, elucidating both atomic structures and their associated band dispersions (ARPES). They are reversible, thanks to the easy malleability of As atoms, being able to transition from one to the other,

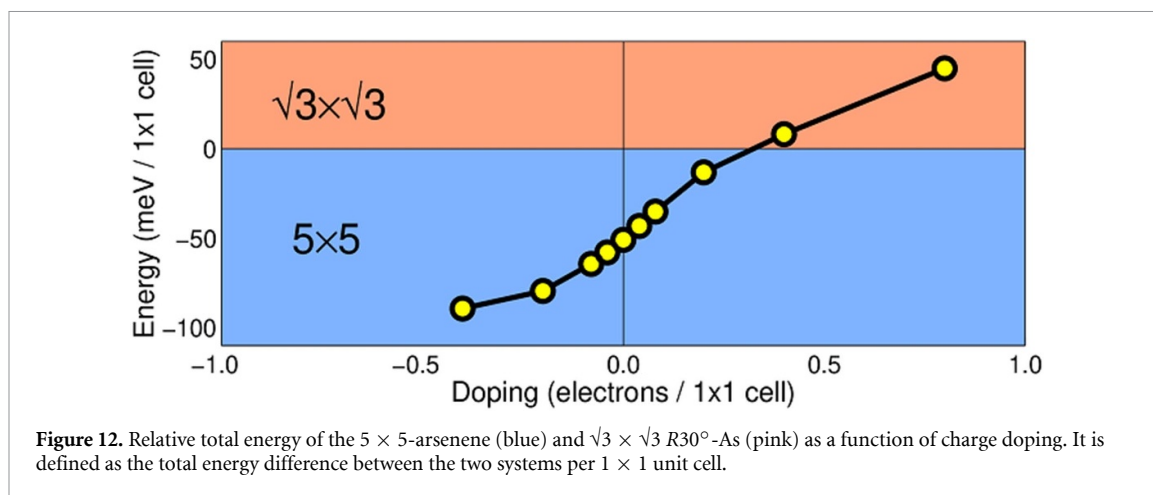


**Figure 12.** Relative total energy of the  $5 \times 5$ -arsenene (blue) and  $\sqrt{3} \times \sqrt{3}$   $R30^\circ$ -As (pink) as a function of charge doping. It is defined as the total energy difference between the two systems per  $1 \times 1$  unit cell.

by applying either temperature or electronic irradiation, keeping the same number of atoms on surface, as determined both experimentally and theoretically.

### Data availability statement

The data that support the findings of this study are available upon reasonable request from the authors.

### Acknowledgment

The authors would like to thank Sandro Priori, Alessandro Ippoliti, and Marco Guaragno for their invaluable technical help.

### Conflicts of interest

The authors declare no conflict of interest.

### ORCID iDs

Paola De Padova  <https://orcid.org/0000-0001-5836-4884>

Carlo Ottaviani  <https://orcid.org/0000-0001-9364-8591>

Bruno Olivieri  <https://orcid.org/0000-0002-3845-3721>

Mariusz Krawiec  <https://orcid.org/0000-0002-8752-4928>

### References

- [1] De Padova P, Larciprete R, Quaresima C, Gunnella R, Reginelli A, Ferrari L, Perfetti P, Yu-Zhang K and Leprince-Wang Y 2001 High resolution photoemission core level spectroscopy study and TEM analysis of the Ge/As/Si(001) growth *Surf. Sci.* **482–485** 574–9
- [2] Novoselov K S, Geim A K, Morozov S V, Jiang D, Zhang Y, Dubonos S V, Grigorieva I V and Firsov A A 2004 Electric field effect in atomically thin carbon films *Science* **306** 666–9
- [3] Vogt P, De Padova P, Quaresima C, Avila J, Frantzeskakis E, Asensio M C, Resta A, Ealet B and Le Lay G 2012 Compelling experimental evidence for graphene like two-dimensional silicon *Phys. Rev. Lett.* **108** 155501–5
- [4] Stpniak-Dybala A, Dyniec P, Kopciuszyski M, Zdyb R, Jalochoowski M and Krawiec M 2019 Planar silicene: a new silicon allotrope epitaxially grown by segregation *Adv. Funct. Mater.* **29** 1906053–5
- [5] Lin C-H *et al* 2018 Single-layer dual germanene phases on Ag(111) *Phys. Rev. Mater.* **2** 024003–8
- [6] Qin Z H, Pan J, Lu S, Shao Y, Wang Y, Du S, Gao H-J and Cao G 2017 Direct evidence of Dirac signature in bilayer germanene islands on Cu(111) *Adv. Mater.* **29** 1606046–5
- [7] Zhang L, Bampoulis P, Rudenko A, Yao Q, van Houselt A, Poelsema B, Katsnelson M and Zandvliet H 2016 Structural and electronic properties of germanene on MoS<sub>2</sub> *Phys. Rev. Lett.* **116** 256804–6
- [8] Derivaz M, Dentel D, Stephan R, Hanf M-C, Mehdaoui A, Sonnet P and Pirri C 2015 Continuous germanene layer on Al(111) *Nano Lett.* **15** 2510–6
- [9] Bampoulis P, Zhang L, Safaei A, van Gastel R, Poelsema B and Zandvliet H J W 2014 Germanene termination of Ge<sub>2</sub>Pt crystals on Ge(110) *J. Phys.: Condens. Matter* **26** 442001–6
- [10] Dávila M E, Xian L, Cahangirov S, Rubio A and Le Lay G 2014 Germanene: a novel two-dimensional germanium allotrope akin to graphene and silicene *New J. Phys.* **16** 095002–10
- [11] Li L, Lu S-Z, Pan J, Qin Z, Wang Y-Q, Wang Y, Cao G-Y, Du S and Gao H-J 2014 Buckled germanene formation on Pt(111) *Adv. Mater.* **26** 4820–4
- [12] Zhu F-F, Chen W-J, Xu Y, Gao C-L, Guan D-D, Liu C-H, Qian D, Zhang S-C and Jia J-F 2015 Epitaxial growth of two-dimensional stanene *Nat. Mater.* **14** 1020–5
- [13] Deng J *et al* 2018 Epitaxial growth of ultraflat stanene with topological band inversion *Nat. Mater.* **17** 1081–7
- [14] Yuhara J, He B, Matsunami N, Nakatake M and Le Lay G 2019 Graphene's latest cousin: plumbene epitaxial growth on a "nano water cube" *Adv. Mater.* **31** 1901017–6
- [15] Bihlmayer G, Sassmannshausen J, Kubetzka A, Blügel S, von Bergmann K and Wiesendanger R 2020 Plumbene on a magnetic substrate: a combined scanning tunneling microscopy and density functional theory study *Phys. Rev. Lett.* **124** 126401–5
- [16] Zhang J L *et al* 2016 Epitaxial growth of single layer blue phosphorus: a new phase of two-dimensional phosphorus *Nano Lett.* **16** 4903–8
- [17] Shah J, Wang W, Sohail H M and Uhrberg R I G 2020 Experimental evidence of monolayer arsenene: an exotic 2D semiconducting materials *2D Mater.* **7** 025013–7
- [18] Lei T, Liu C, Zhao J-L, Li J-M, Li Y-P, Wang J-O, Wu R, Qian H-J, Wang H-Q and Ibrahim K 2016 Electronic structure of antimonene grown on Sb<sub>2</sub>Te<sub>3</sub>(111) and Bi<sub>2</sub>Te<sub>3</sub> substrates *J. Appl. Phys.* **119** 015302–5

- [19] Wu X *et al* 2017 Epitaxial growth and air-stability of monolayer antimonene on PdTe<sub>2</sub> *Adv. Mater.* **29** 1605407–6
- [20] Reis F, Li G, Dudy L, Bauernfeind M, Glass S, Hanke W, Thomale R, Schäfer J and Claessen R 2017 Bismuthene on a SiC substrate: a candidate for a high-temperature quantum spin Hall material *Science* **357** 287–4
- [21] Li L, Wang Y, Xie S, Li X-B, Wang Y-Q, Wu R, Sun H, Zhang S and Gao H-J 2013 Two-dimensional transition metal honeycomb realized: Hf on Ir(111) *Nano Lett.* **3** 4671–4
- [22] Mannix A J *et al* 2015 Synthesis of borophenes: anisotropic, two-dimensional boron polymorphs *Science* **350** 1513–6
- [23] Feng B, Zhang J, Zhong Q, Li W, Li S, Li H, Cheng P, Meng S, Chen L and Wu K 2016 Experimental realization of two-dimensional boron sheets *Nat. Chem.* **8** 563–8
- [24] Liu X, Zhang Z, Wang L, Yakobson B I and Hersam M C 2018 Intermixing and periodic self-assembly of borophene line defects *Nat. Mater.* **17** 783–6
- [25] Zhang H-M *et al* 2015 Detection of a superconducting phase in a two-atom layer of hexagonal Ga film grown on semiconducting GaN(0001) *Phys. Rev. Lett.* **114** 107003–5
- [26] Qin J *et al* 2017 Controlled growth of a large-size 2D selenium nanosheet and Its electronic and optoelectronic applications *ACS Nano* **11** 10222–9
- [27] Zhu Z *et al* 2017 Multivalency-driven formation of Te-based monolayer materials: a combined first-principles and experimental study *Phys. Rev. Lett.* **119** 106101–5
- [28] Yi Y, Li Z, Cao S, Han J and Zhang Z 2025 Geometrical stability, electrical contact and optical properties for ZrX<sub>2</sub>(X = Cl, Br, I) /Zr<sub>2</sub>Cl<sub>2</sub> semiconductor-metal heterojunctions *Appl. Surf. Sci.* **682** 161730–13
- [29] Li Z, Han J, Cao S, Zhang Z and Deng X 2023 Physical properties of monolayer Mn(BiTeS)<sub>2</sub> and its applications in sub-3 nm spintronic devices *Phys. Rev. B* **108** 184413–5
- [30] Zhu Z, Guan J and Tománek D 2015 Strain-induced metal-semiconductor transition in monolayers and bilayers of gray arsenic: a computational study *Phys. Rev. B* **91** 161404(R)–5
- [31] Kamal C and Ezawa M 2015 Arsenene: two-dimensional buckled and puckered honeycomb arsenic systems *Phys. Rev. B* **91** 085423–10
- [32] Wang G, Pandey R and Karna S P 2015 Atomically thin group v elemental films: theoretical investigations of antimonene allotropes *ACS Appl. Mater. Interfaces* **7** 11490–6
- [33] Gupta S K, Sonvane Y, Wang G and Pandey R 2015 Size and edge roughness effects on thermal conductivity of pristine antimonene allotropes *Chem. Phys. Lett.* **641** 169–72
- [34] Zhang S, Xie M, Li F, Yan Z, Li Y, Kan E, Liu W, Chen Z and Zeng H 2016 Semiconducting group 15 monolayers: a broad range of band gaps and high carrier mobilities *Angew. Chem.* **128** 1666–9
- [35] Zhang S, Guo S, Chen Z, Wang Y, Gao H, Gómez-Herrero J, Ares P, Zamora F, Zhu Z and Zeng H 2018 Recent progress in 2D group-VA semiconductors: from theory to experiment *Chem. Soc. Rev.* **47** 982–1021
- [36] Norman N C (ed) 1997 *Chemistry of Arsenic, Antimony and Bismuth* (Springer)
- [37] Welles A F 1982 *Structural Inorganic Chemistry* 5th edn (Clarendon Press, Oxford University Press)
- [38] Madelung O 2004 *Semiconductors: Data Handbook* 3rd edn (Springer)
- [39] Rahman G, Mahmood A and García-Suárez V M 2019 Dynamically stable topological phase of arsenene *Sci. Rep.* **9** 7966
- [40] Zhang S, Yan Z, Li Y, Chen Z and Zeng H 2015 Atomically thin arsenene and antimonene: semimetal–semiconductor and indirect–direct band-gap transitions *Angew. Chem.* **127** 3155–8
- [41] Vishnoi P, Mazumder M, Pati S K and R. Rao C N 2018 Arsenene nanosheets and nanodots *New J. Chem.* **42** 14091–5
- [42] Yu Q, Chen C, Guo K, Deng H, Yi T, Zhang Y, Su W, Wu J and Zhang K 2021 Deterministic transfer of large-scale  $\beta$ -phase arsenic on fiber end cap for near-infrared ultrafast pulse generation *Front. Mater.* **8** 721587
- [43] Shah J, Wang W, Sohail H M and Uhrberg R 2020 Quasi one-dimensional structure formed by an As/Ag(111) surface alloy *J. Phys. Chem. C* **124** 24196–203
- [44] Perdew J P, Burke K and Ernzerhof M 1996 Generalized gradient approximation made simple *Phys. Rev. Lett.* **77** 3865–8
- [45] Kresse G and Furthmüller J 1996 Efficient iterative schemes for ab initio total-energy calculations using a plane-wave basis set *Phys. Rev. B* **54** 11169–86
- [46] Kresse G and Joubert D 1999 From ultrasoft pseudopotentials to the projector augmented-wave method *Phys. Rev. B* **59** 1758–75
- [47] Blöchl P E 1994 Projector augmented wave method *Phys. Rev. B* **50** 17953–79
- [48] Monkhorst H J and Pack J D 1976 Special points for Brillouin-zone integrations *Phys. Rev. B* **13** 5188–92
- [49] Pantano C G and Madey T E 1981 Electron beam damage in Auger electron spectroscopy *Appl. Surf. Sci.* **7** 115–41
- [50] Brown A and Rundqvist S 1965 Refinement of the crystal structure of black phosphorus *Acta Crystallogr.* **19** 684–5
- [51] Hultgren R, Gingrich N S and Warren B E 1935 The atomic distribution in red and black phosphorus and the crystal structure of black phosphorus *J. Chem. Phys.* **135** 351–5